NASA Technical Memorandum 81828

Longitudinal Stability and Control in Wind Shear With Energy Height Rate Feedback

Joseph Gera

NOVEMBER 1980

NASA

NASA Technical Memorandum 81828

Longitudinal Stability and Control in Wind Shear With Energy Height Rate Feedback

Joseph Gera
Langley Research Center
Hampton, Virginia

National Aeronautics
and Space Administration

**Scientific and Technical
Information Branch**

1980

SUMMARY

The longitudinal linearized equations of motion in wind shear have been derived for the NASA Terminal Configured Vehicle, a modified Boeing 737 airplane. In addition to the apparent acceleration terms due to wind shear, the equations include altitude-dependent stability derivatives. A linear analysis of these equations indicates a first-order divergence type of instability due to wind shear in which head wind decreases with altitude. Furthermore, this instability cannot be stabilized by attitude control alone. However, attitude control used in combination with an additional feedback loop which consists of the energy height rate feedback to the throttle proved to be effective in suppressing instability due to wind shear. In the present report the term "energy height" denotes the sum of kinetic and potential energies per unit weight of the airplane referenced to the surrounding air mass. A brief piloted, real-time, nonlinear simulation indicated the desirability of using a display based on the rate of change of energy height and of commanded thrust.

INTRODUCTION

The effect of wind shear on aircraft trajectories and aircraft control has been the subject of numerous studies dealing with aviation safety. These studies are usually conducted on complex simulations of specific aircraft with an assumed atmospheric wind model which includes a particular variation of the wind as a function of Earth-fixed coordinates. In contrast, references 1 and 2 deal with the effect of wind shear on the longitudinal stability and control within the framework of a small-disturbance theory of flight dynamics. The analysis presented here is an extension of the method proposed in reference 1, in that it includes stability derivatives with respect to height in addition to the kinematic effects of wind shear.

In the mathematical model chosen for the study, the parameters were those of the Boeing 737-100 airplane currently used in the NASA Terminal Configured Vehicle (TCV) Program. A linear variation of the wind magnitude with height was assumed in the analysis. This assumption may limit the applicability of the results, since actual flight experience indicates that not only the magnitude, but also the direction, of the wind may change with altitude. Such changes are also frequently accompanied by sustained updrafts and downdrafts. Although a rigorous treatment of the effect of these types of atmospheric motion on longitudinal stability is beyond the scope of the present analysis, the control law proposed here for alleviating the effects of linear wind shear is shown to be useful in alleviating the effects of updrafts and downdrafts.

SYMBOLS

Values are given in both SI and U.S. Customary Units. Measurements were made in U.S. Customary Units.

A	coefficient matrix in linear equations of motion
B	control matrix in linear equations of motion
C_L	lift coefficient
$C_{L_{\dot{\alpha}}}$	nondimensional rotary stability derivative, $\partial C_L / \partial(\bar{c}\dot{\alpha}/2V)$
C_m	pitching-moment coefficient
$C_{m_{\dot{\alpha}}}$	nondimensional rotary stability derivative, $\partial C_m / \partial(\bar{c}\dot{\alpha}/2V)$
$\bar{c}$	mean aerodynamic chord, 3.41 m (11.2 ft)
D	aerodynamic drag, N (lbf)
D_V	$= \frac{\partial D}{\partial V}$, kg/sec (slugs/sec)
D_α	$= \frac{\partial D}{\partial \alpha}$, kg-m/sec^2 (slug-ft/sec^2)
D_{δ_e}	$= \frac{\partial D}{\partial \delta_e}$, N/deg (lbf/deg)
D_{δ_T}	$= \frac{\partial D}{\partial (\delta_T)}$
F_x, F_z	total force components in the direction of x- and z-wind axes, respectively, N (lbf)
g	gravitational acceleration, 9.81 m/sec^2 (32.2 ft/sec^2)
h	altitude above mean sea level, m (ft)
h_e	energy height, $\frac{V^2}{2g} + h$, m (ft)
$Im(s)$	imaginary part of complex variable
I_{yy}	moment of inertia, kg-m^2 (slug-ft^2)
$K_{\dot{h}_e}$	proportional gain, deg/(m/sec) (deg/(ft/sec))
K_I	integral gain, deg/m (deg/ft)

K_θ gain on pitch rate to elevator, deg/deg

L aerodynamic lift, N (lbf)

L_q $= \frac{\partial L}{\partial q}$, N-sec (lbf-sec)

L_V $= \frac{\partial L}{\partial V}$, kg/sec (slugs/sec)

L_α $= \frac{\partial L}{\partial \alpha}$, kg-m/sec^2 (slug-ft/sec^2)

$L_{\dot{\alpha}}$ $= \frac{\partial L}{\partial \dot{\alpha}}$, kg-m/sec (slug-ft/sec)

L_{δ_e} $= \frac{\partial L}{\partial \delta_e}$, N/deg (lbf/deg)

M aerodynamic pitching moment, N-m (lbf-ft)

M_q $= \frac{\partial M}{\partial q}$, kg-m^2/sec (slug-ft^2/sec)

M_V $= \frac{\partial M}{\partial V}$, kg-m/sec (slug-ft/sec)

M_α $= \frac{\partial M}{\partial \alpha}$, kg-m^2/sec^2 (slug-ft^2/sec^2)

$M_{\dot{\alpha}}$ $= \frac{\partial M}{\partial \dot{\alpha}}$, kg-m^2/sec (slug-ft^2/sec)

M_{δ_e} $= \frac{\partial M}{\partial \delta_e}$, kg-m^2/(sec^2-deg) (slug-ft^2/(sec^2-deg))

$M_{\delta T}$ $= \frac{\partial M}{\partial (\delta T)}$, m (ft)

m mass, kg (slugs)

q	pitching velocity about body Y-axis, rad/sec
q_w	pitching velocity about wind y-axis, rad/sec
Re(s)	real part of complex variable
S	reference area, m^2 (ft^2)
s	variable in Laplace transformation, sec^{-1}
T	total thrust, N (lbf)
T_e	trim value of thrust, N (lbf)
T_V	$= \frac{\partial T}{\partial V}$, kg/sec (slugs/sec)
t	time, sec
u_w	magnitude of horizontal wind, m/sec (ft/sec)
u_w'	$= \frac{du_w}{dz_E}$, sec^{-1}
V	total velocity relative to moving air mass, m/sec (knots)
V_e	equilibrium velocity relative to moving air mass, m/sec (knots)
v_w	magnitude of lateral wind, m/sec (ft/sec)
w_w	magnitude of vertical wind, m/sec (ft/sec)
Z_E	Earth-fixed Z-coordinate, m (ft)
α	angle between zero lift line and relative wind vector, rad
α_e	trim value of angle of attack, rad
α_T	angle between thrust line and zero lift line, rad
γ	angle between local horizontal and relative wind, rad
γ_e	equilibrium or trim value of γ, rad
Δh	perturbation in altitude from the initial condition, m (ft)
ΔV	perturbation in relative wind, m/sec (ft/sec)
ΔZ_E	perturbation in Z_E-coordinate, m (ft)

$\Delta\alpha$	perturbation angle of attack, rad
$\Delta\gamma$	perturbation in relative flight-path angle, rad
$\Delta\theta$	perturbation in pitch attitude, rad
δ_e	elevator deflection measured from trim value, deg
$\delta_{e,p}$	elevator command from pilot, deg
$\delta_{e,STAB}$	trim value of stabilizer position, deg
δT	thrust perturbation measured from trim value, N (lbf)
δ_{th}	throttle position, deg
$\delta_{th,c}$	throttle position command, deg
θ	pitch attitude, deg
θ_{ref}	reference value of pitch attitude, deg
θ_w	Euler angle of x-wind axis measured from Earth-fixed X-axis, deg
ζ_p, ζ_{sp}	damping ratio of phugoid and short-period modes, respectively
ω_p, ω_{sp}	undamped natural frequency of phugoid and short-period modes, respectively, rad/sec

A dot over a symbol denotes the first derivative taken with respect to time.

MODEL DEFINITION

In this section, the wind is defined by the same simple linear relationship which was used in reference 1:

$$u_W = u_W' z_E \tag{1}$$

where $u_W' = \dfrac{du_W}{dz_E}$

$$v_W = 0 \tag{2}$$

$$w_W = 0 \tag{3}$$

That is, the only nonzero component of the wind lies in the horizontal plane, parallel to the Earth-fixed X-axis, and this component varies linearly with the Earth-fixed Z-coordinate Z_E. By definition, u_w is positive in the case of a tail wind. In all cases the wind gradient u_w' will be considered a constant. Figure 1 illustrates the definition of the axis systems and the wind gradient.

The airplane is represented by a longitudinal small-disturbance model wherein wind axes are used for the lift-force and drag-force equations, and body axes for the pitching-moment equation. The small-disturbance model is obtained by linearizing about an equilibrium path the following nonlinear equations of motion:

$$m(\dot{V} - Vu_w' \sin \theta_w \cos \theta_w) = F_X \tag{4}$$

$$m(-Vq_w - Vu_w' \sin^2 \theta_w) = F_Z \tag{5}$$

$$I_{yy}\dot{q} = M \tag{6}$$

The derivation of these equations is presented, with minor differences in notation, in reference 1.

The equilibrium flight path is taken to be a path along which $\dot{V}$, q_w, and $\dot{q}$ are equal to zero. Since

$$q_w = q - \dot{\alpha} \tag{7}$$

the steady-state flight path is seen to be either level flight, steady climb, or dive with fixed controls. Although this flight path corresponds to generally accepted notions about flight in a steady state, reference 1 shows that the definition just given of steady state allows flight paths which do not appear rectilinear for an observer fixed to an inertial reference frame.

Except for the terms due to the wind shear, equations (4), (5), and (6) are those given in standard textbooks on airplane stability and control. Consequently, the reader is referred to reference 3 (pp. 157-163) for details of the linearization. The additional acceleration terms which appear on the left-hand side of equations (4) and (5) can be easily linearized. Since this report deals with two-dimensional motion, the symbol θ_w denoting the flight-path angle is replaced by the more conventional symbol γ. A Taylor series expansion to the first order results in the following expressions of the terms which contain the wind gradient:

$$Vu_w' \sin\gamma \cos\gamma = V_e u_w' \sin\gamma_e \cos\gamma_e + \left(\frac{1}{2} u_w' \sin 2\gamma_e\right) \Delta V + (V_e u_w' \cos 2\gamma_e)\ \Delta\gamma \tag{8}$$

$$Vu_w' \sin^2\gamma = V_e u_w' \sin^2\gamma_e + (u_w' \sin^2\gamma_e)\ \Delta V + (V_e u_w' \sin 2\gamma_e)\ \Delta\gamma \tag{9}$$

where the higher order terms have been omitted and the following convention has been used:

$$V = V_e + \Delta V \tag{10}$$

$$\gamma = \gamma_e + \Delta\gamma \tag{11}$$

Thus, the presence of wind shear modifies Etkin's linearization by the addition of the equilibrium or trim terms

$$-V_e u_w' \sin\gamma_e \cos\gamma_e$$

and

$$-V_e u_w' \sin^2\gamma_e$$

to the equations describing the trimmed flight. Also, the linearized drag-force and lift-force equations of Etkin (ref. 3, p. 163) must include the following terms which result from wind shear:

Drag-force equation:

$$\left(\frac{1}{2} u_w' \sin 2\gamma_e\right) \Delta V - (V_e u_w' \cos 2\gamma_e)\ \Delta\alpha + (V_e u_w' \cos 2\gamma_e)\ \Delta\theta$$

Lift-force equation:

$$(u_w' \sin^2\gamma_e)\ \Delta V - (V_e u_w' \sin 2\gamma_e)\ \Delta\alpha + (V_e u_w' \sin 2\gamma_e)\ \Delta\theta$$

Stability Derivatives Due to Altitude Change

These derivatives are normally neglected because most linear analyses assume the atmosphere to be uniform. In the present analysis, however, these Z_E-derivatives naturally arise since the wind speed varies with the Z_E-coordinate. However, the Z_E-derivatives will be included in the analysis only for the case of horizontal, wings-level, trimmed flight; i.e., the analysis will consider only two cases:

1. $\gamma_e = 0$ and Z_E-derivatives are nonzero
2. $\gamma_e \neq 0$ and Z_E-derivatives are assumed to be zero

The Z_E-derivatives $\frac{\partial F_x}{Z_E}$, $\frac{\partial F_z}{Z_E}$, and $\frac{\partial M}{\partial Z_E}$ are evaluated as

$$\frac{\partial F_x}{\partial Z_E} = \frac{\partial F_x}{\partial u_w}\frac{\partial u_w}{\partial Z_E} = -\frac{\partial F_x}{\partial V}u_w' \tag{12}$$

$$\frac{\partial F_z}{\partial Z_E} = \frac{\partial F_z}{\partial u_w}\frac{\partial u_w}{\partial Z_E} = -\frac{\partial F_z}{\partial V}u_w' \tag{13}$$

$$\frac{\partial M}{\partial Z_E} = \frac{\partial M}{\partial u_w}\frac{\partial u_w}{\partial Z_E} = -\frac{\partial M}{\partial V}u_w' \tag{14}$$

This is, for horizontal flight, the Z_E-derivatives can be obtained very simply from the conventional speed-derivatives if the wind gradient u_w' is known. For diving or climbing flight, the evaluation of these derivatives would be much more complicated because of their dependence on altitude, flight-path angle, atmospheric density, etc.

Thus, the longitudinal equations of motion of an airplane flying in a vertical wind gradient can be composed from the conventional small-disturbance equations by adding certain kinematic terms and the Z_E-derivatives. For the sake of completeness, both the conventional and wind shear terms are given in their literal form in the appendix.

Linearized Equations of Motion of the TCV Airplane

The specific airplane selected for the analysis is the NASA Terminal Configured Vehicle (TCV), which is a modified Boeing 737. The linear equations

of motion were evaluated in level flight and in a 3^{o} descent at the flight conditions described in table I (vehicle parameters are also described).

TABLE I.- FLIGHT CONDITIONS AND VEHICLE PARAMETERS

Altitude, m (ft)	152.4 (500)
Equivalent airspeed, m/sec (knots)	64.77 (125)
Weight, kN (lbf)	378 (85 000)
I_{yy}, kg-m^2 (slug-ft^2)	1.08×10^6 (7.99×10^5)
Gear	Down
Flaps, deg	40
Reference area, m^2 (ft^2)	91.04 (980)
Mean aerodynamic chord c, m (ft)	3.41 (11.2)
Center of gravity, percent c	18

The coefficient matrices of the linearized equations of motion are listed in the appendix. The matrices were computed for the no-shear case by using the computer program described in reference 4. Wind shear effects were included by adding both the kinematic terms and the Z_E-derivatives to the computed matrices. In table II trim values of the more important vehicle parameters are listed.

TABLE II.- TRIM VALUES OF THE TCV AIRPLANE PARAMETERS

Parameter	$\gamma_e = 0^o$	$\gamma_e = -3^o$
V_e, m/sec (knots)	64.77 (125)	64.77 (125)
α_e, deg	2.28	2.38
T_e, kN (lbf)	57.6 (13 174)	38.1 (8712)
$\delta_{e,STAB}$, deg	8.37	8.34
δ_e, deg	2.76	2.54

EFFECT OF WIND SHEAR ON THE BASIC AIPRLANE

The longitudinal motion of the basic airplane in the absence of wind shear is characterized by an adequately damped short-period mode (ω_{sp} = 1.35 rad/sec; ζ_{sp} = 0.46) and a lightly damped phugoid mode (ω_p = 0.166 rad/sec; ζ_p = 0.08). As shown in reference 1, the principal effect of the type of wind shear assumed here is reflected in the phugoid motion of conventional aircraft. This was certainly the case for the TCV airplane. Varying the wind gradient u_w' between -0.1 sec^{-1} and 0.1 sec^{-1} had an insignificant effect on the short-period mode. The effect of varying u_w' on the phugoid characteristics is depicted in the

root contours shown in figure 2 for $\gamma_e = 0^o$ and $\gamma_e = -3^o$. There is a significant difference between the two contours, especially for positive values of u_w'. If u_w' exceeds approximately 0.07, the oscillatory phugoid root splits into a subsidence and a divergence or "tuck" mode. An additional pole, due to the coupled Z_E-equation in the $\gamma_e = 0^o$ case, remains close to the origin at all values of u_w'; hence, this pole is not shown.

The difference between the two contours (shown in fig. 2) may be attributed to either of two factors: the different values of γ_e or the presence or absence of the Z_E-derivatives. To resolve this question, the root contour was computed for the $\gamma_e = 0$ case, but with all Z_E-derivatives set equal to zero. The result is shown in figure 3 along with the original $\gamma_e = 0$ contour reproduced from figure 2. The influence of the Z_E-derivatives on the equations of motion is much greater than the influence of γ_e. In the computation of the poles for the $\gamma_e = 0$ case in the presence of wind shear, the following observation (pointed out by Windsor L. Sherman, of the Langley Research Center) can be made: The shift in the location of the poles in the complex plane is the same whether the shift is due to the Z_E-derivatives or to the additional acceleration terms in equations (8) and (9).

For purposes of comparison, time histories were computed for the $\gamma_e = 0$ cases with three values of the wind gradient u_w'. The values selected were $u_w' = 0$, i.e., no shear, and $u_w' = \pm 1$ sec^{-1}. The latter values correspond to very large shear, and it is unlikely that wind shears of this magnitude occur in an atmospheric layer thick enough for the airplane to achieve equilibrium. These extremes were chosen to demonstrate clearly the effect of wind shear on the motion. Figure 4 illustrates the controls-fixed response of the airplane to an initial step tail wind gust of 3 m/sec. In comparison with the no-shear ($u_w' = 0$) case, and the case in which head wind increases with decreasing altitude ($u_w' = -1$), the traces showing the motion in a wind shear when $u_w' = 1$ reveal the following information about the latter type of shear. Up to about 14 sec into the time histories, shear of this type is accompanied by both an airspeed and an altitude loss caused by the initial disturbance. The $u_w' = 1$ case clearly shows the divergence or "tuck" mode due to wind shear. It should be pointed out that the time histories were computed with the controls fixed; normally, the pilot would not allow the large speed or altitude excursions to occur.

Attitude Control in Wind Shear

The simplest form of attitude control is the feedback of pitch attitude θ to the elevator δ_e through a pure gain K_θ, as shown schematically in figure 5. The root locii presented in figure 6 depict the closed-loop characteristics of this type of control under the same three types of wind shear conditions for which the time histories were computed in the previous section:

1. Head wind decreasing with altitude gain, $u_w' = -1$
2. No wind shear, $u_w' = 0$
3. Head wind increasing with altitude gain, $u_w' = 1$

All three root locii show qualitatively that the θ to δ_e feedback does not add additional damping to the system; it merely redistributes the total available damping between the short-period and the phugoid modes, as reflected in the fact that the sum of all the poles does not vary significantly as the gain is changed. Figure 6(c) shows the existence of a nonminimum phase zero in wind shear where $u_w' = 1$. This means that an instability will exist for any value of the gain K_θ so that neither the pilot nor an attitude feedback control system could stabilize the first-order divergent mode by pitch attitude closure alone.

Energy Considerations

The energy balance of the airplane is affected by the variation of horizontal wind. This can be shown by multiplying the drag equation by V and noting that $\dot{h} = V \sin \gamma$. The resulting energy relationship

$$\frac{d}{dt}\left(\frac{1}{2g} V^2 + h\right) = \frac{V}{mg}(T \cos \alpha - D) + \frac{V^2}{g} u_w' \sin \gamma \cos \gamma$$

shows that the rate of energy change per unit weight computed relative to the surrounding air mass, sometimes denoted by h_e, or energy height, is equal to the specific excess power $\frac{V}{mg}(T \cos \alpha - D)$ plus a term due to the wind shear. Note that the wind shear term $\frac{V^2}{g} u_w' \sin \gamma \cos \gamma$ can take either a positive or a negative sign. During a landing approach, when $\gamma < 0$, the shear in which $u_w' > 0$ results in an excessive decrease of energy height which is due to wind shear only. The loss of energy is further aggravated by the ineffectiveness of attitude control in stabilizing the first-order divergence (as shown in the preceding section).

Examination of the foregoing energy equation suggests a possible method to cancel the wind shear term as reported by Joppa in reference 5. If specific excess power is assumed constant, the presence of wind shear would be indicated by a change in the energy height rate. This also means that it should be possible to vary the thrust term in such a way as to keep the energy rate constant regardless of the sign and magnitude of the wind shear term. At constant airspeed, of course, the energy height rate is just the rate of climb/descent. If approach and landing take place while the airplane is flying on the back side of the drag polar, pilots generally control rate descent by adjusting the throttle setting. Thus, the closure of energy height rate to throttle appears to be a natural choice from the standpoint of both the energy balance of the airplane and manual control techniques during landing. Reference 6 describes a practical, inexpensive method of airborne energy height measurement which is the subject of research studies at the Langley Research Center.

Closed-loop Control of Energy Height Rate

In this section, it is assumed that the pilot controls pitch attitude by the elevator; thus, the pitch attitude to elevator control loop remained closed in the manner previously described with $K_\theta = 0.32$. While this choice was somewhat arbitrary, it resulted in a satisfactory short-period damping ratio of approximately 0.4 for all three wind gradient cases:

$$u_w' = -1$$

$$u_w' = 0$$

$$u_w' = 1$$

For the first two cases, this choice of K_θ also increased the phugoid damping, but the $u_w' = 1$ case still had the unstable divergent mode. Stabilization of the latter was attempted by closing the energy height rate throttle loop through the following transfer function:

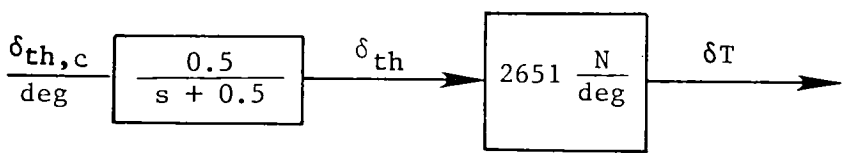

The preceding linear gain-lag combination represents an adequate approximation of the TCV airplane power plant at the flight condition specified in table II. Figure 7 shows the closed-loop configuration examined in the subsequent paragraphs. The configuration includes a forward-loop integration which was intended to improve the low-frequency characteristics of the $\dot{h}_e$ loop. Figure 8 shows the root locii for the three values of u_w' without the forward-loop integration. Energy height rate feedback is seen to stabilize the unstable mode due to wind shear while leaving the short-period characteristics virtually unchanged. The only adverse effect of $\dot{h}_e$ feedback is on the phugoid mode at $u_w' = -1$. As the gain $K_{\dot{h}_e}$ approaches infinity, the phugoid pole closes on a zero in the right-hand half-plane. Figure 9 shows the same three root locii with a forward-loop integration and K_I equal to $\frac{1}{5} K_{\dot{h}_e}$. For moderate values of the gain, say $0.4 < K_{\dot{h}_e} < 0.5$, both the augmented short-period and phugoid modes possess acceptable characteristics with or without forward-loop integration. Time histories of several motion variables as well as those of the elevator and throttle are presented in figures 10 and 11 for the closed-loop case $K_I = 0.1$ and $K_{\dot{h}_e} = 0.5$.

Piloted Simulation of Energy Height Rate Control

In the preceding linear analysis, the effectiveness of $\dot{h}_e$ feedback was shown in stabilizing the divergent mode in the wind shear in which $u_w' = 1$. In order to show that this feedback is also effective in controlling the flight path during nonlevel flight and in a more realistic wind shear environment, a brief piloted simulation was conducted using a large-scale, nonlinear simulation of the TCV airplane and the aft flight deck. For a detailed description of this simulation, see reference 7.

In the simulation, the pilot's task was to make an instrument approach on a 3^o glide slope using either an experimental attitude control wheel steering mode or a fully coupled automatic landing mode to apply elevator commands. Simultaneously, he controlled engine thrust by making throttle commands either through a manual, proportional system or through an engine height rate control system in which power lever position was proportional to energy height rate.

A simplified schematic of the control modes is shown in figure 12. The details of the elevator control modes are not shown because the objective of the simulation was the comparison of manual throttle control with the energy height rate system from the standpoint of pilot work load during wind shear conditions. The simulated wind profile (shown in fig. 13) included not only a variation of the horizontal wind with altitude, but also two separate regions of strong downdrafts.

A typical approach using the autoland control mode for elevator control with manual control of the throttles is shown in figure 14. The task consisted of a straight-in approach in approximately level flight until the glide slope was intercepted at an altitude of approximately 300 m (1000 ft). Thereafter, the pilot attempted to maintain airspeed at 120 knots by manipulating the throttles. The magnitude of $\dot{h}_e$ was not displayed to the pilot. The time histories show the coupling existing between the power setting and the energy height rate. The minimum value of the energy height rate occurred at about 42 sec, approximately 150 m (490 ft) altitude, as a result of reducing the throttle setting about 10 sec earlier. Noting the loss of airspeed, the pilot then rapidly advanced the throttles to almost full power. The autoland mode almost simultaneously commanded a nose-down elevator of about 4^o. Despite the nose-down command the airspeed continued to fall, and the rate of descent increased, because of the decreasing headwind and the increasing downdraft for about 20 sec. The energy height rate trace also reflects the combined effect of the horizontal and vertical wind. Subsequently, as the downdraft abated and the throttle setting remained very high, the energy height rate reached its maximum, and airspeed increased significantly. Eventually a relatively smooth touchdown with a vertical velocity of 0.6 m/sec (2 ft/sec) was made by the autoland system. These results should be compared with figure 15 which depicts time histories obtained under the same conditions; the throttles, however, were driven completely by the energy height rate system except for manually repositioning the throttle levers at the time of glide slope interception and at flare initiation. (It is significant that during the approach the pilot did not manipulate the throttles manually except initially and during flare.) As expected, the energy height trace is much smoother than during the previous run, and the value of $\dot{h}_e$ gradually increased from the minimum as the downdraft abated and

the horizontal wind became constant. The increase in $\dot{h}_e$ resulted in a decreased power setting just before initiating flare. At the expense of the airspeed momentarily falling below 105 knots, the large airspeed increase which had been experienced during manual throttle operation at this point on the approach trajectory was avoided. The approach resulted in a touchdown similar to that of the previous case. Detailed comparison of the two approaches indicates that the use of an energy height rate system in the throttle loop results in an approach very similar to and in some respects slightly better than that obtained with manual throttle. The significant point, however, is that pilot work load was reduced with the energy height rate system.

Figure 16 shows an approach flown with attitude-control-wheel steering mode in the elevator loop and energy height rate system in the throttle loop. This combination resulted in a significantly higher pilot work load than what was experienced with the autoland and energy height rate combination. Also, in terms of glide slope error and vertical velocity at touchdown, this approach trajectory was inferior to those of the previous two cases. The pilot stated that the effects of wind shear and downdraft made the pitch axis control difficult to recognize as an attitude control system. In the opinion of the pilot, manual throttle operation in combination with experimental control wheel steering mode would have been completely unacceptable.

However, despite its beneficial effect in reducing the pilot work load in wind shear, the pilot expressed dislike of the throttle loop augmentation by the $\dot{h}_e$ signal when used either with the autoland or the experimental attitude control modes. The reason stated was that manual throttle commands would be canceled or overridden by the $\dot{h}_e$ feedback, resulting in the objectionable impression that the engines were running out of control. Excessive throttle activity would also preclude the operational use of an automatic $\dot{h}_e$ to δT loop.

Consequently, it is postulated that use of the $\dot{h}_e$ signal for energy management during operation in wind shear or up/down drafts could best be accomplished by displaying the output of the energy height rate device for use in manually positioning the throttles. The pilot would then be free to follow or disregard its output. A conceptual display for this purpose is depicted schematically in figure 17. Typical use of this display is as follows: Prior to activating the display, the pilot would null the indicator while flying on the desired flight path at the appropriate power setting. After pulling out the RESET knob, the pilot keeps the indicator at the null position by appropriately positioning the throttle. As used in this mode, the display serves to alert the pilot to the presence of wind shear but leaves him the responsibility of deciding whether to go around or to continue the approach using the output of the display as a guide to modulating the throttle position. Further simulation studies are needed to determine both the display format and its optimum use during the landing approach.

CONCLUDING REMARKS

The longitudinal linearized equations of motion have been derived for the Terminal Configured Vehicle (TCV) Boeing 737 airplane and contain not only the

apparent acceleration terms due to wind shear, but also some altitude-dependent stability derivatives. The inclusion of the latter derivatives amplifies the effects of wind shear on the longitudinal modal characteristics. These wind shear effects, which have been derived in the general case previously, are also true for the TCV airplane.

In the case of the airplane flying with fixed controls, the type of shear in which head wind is decreasing with decreasing altitude results in a first-order divergence. Wind shear in which the head wind increases with decreasing altitude results in decreased damping ratio and increased frequency of the phugoid motion.

The short-period characteristics remain virtually unaffected in both kinds of wind shear.

The phugoid mode instability due to wind shear cannot be stabilized by attitude feedback to the elevator for the TCV airplane; however, adding an energy height rate loop to the throttle resulted in a stable phugoid for the types of wind shear considered in the analysis.

A brief piloted simulation was conducted subsequent to the linear analysis, largely to verify the results of the latter in a large-scale, nonlinear simulation of the TCV airplane. The results are of a preliminary nature, but they do substantiate the findings of the linear analysis. The piloted simulation also indicated that the energy height rate to throttle closure should be made through the pilot utilizing a display. Further simulation effort is needed to arrive at the most suitable form of this display.

Langley Research Center
National Aeronautics and Space Administration
Hampton, VA 23665
August 4, 1980

APPENDIX

LITERAL AND NUMERICAL FORM OF THE COEFFICIENT MATRICES

The longitudinal small-disturbance equations of motion can be written as

$$\dot{\underset{\sim}{x}} = A\underset{\sim}{x} + B\underset{\sim}{u}$$

where the variable $\underset{\sim}{x}$ is the five-dimensional state vector:

$$\underset{\sim}{x} = (\Delta V, \quad \Delta\alpha, \quad q, \quad \Delta\theta, \quad \Delta z_E)$$

and the variable $\underset{\sim}{u}$ is the two-dimensional control vector:

$$\underset{\sim}{u} = (\delta T, \quad \delta_e)$$

The literal forms of the element of the matrices A and B are listed below, giving both the conventional terms (ref. 3) and the terms which must be added if wind shear is included in the analysis. The wind shear contribution included the newly derived altitude-dependent derivatives (e.g., A_{15}, A_{25}, A_{35}):

Altitude-dependent derivatives	Conventional term	Wind shear contribution
A_{11}	$\frac{1}{m}(T_V \cos \alpha_T - D_V)$	$\frac{1}{2} u_w' \sin 2\gamma_e$
A_{12}	$g \cos \gamma_e - \frac{1}{m}(T_e \sin \alpha_T + D_\alpha)$	$-u_w' V_e \cos 2\gamma_e$
A_{13}	0	0
A_{14}	$-g \cos \gamma_e$	$u_w' V_e \cos 2\gamma_e$
A_{15}	0	$-\frac{1}{m}(T_V \cos \alpha_T - D_V) u_w'$ (zero if $\gamma_e \neq 0$)
A_{21}	$-\frac{L_V + T_V \sin \alpha_T}{mV_e + L_{\dot{\alpha}}}$	$\frac{m u_w' \sin^2 \gamma_e}{mV_e + L_{\dot{\alpha}}}$
A_{22}	$-\frac{L_\alpha + T_e \cos \alpha_T - mg \sin \gamma_e}{mV_e + L_{\dot{\alpha}}}$	$-\frac{m u_w' V_e \sin 2\gamma_e}{mV_e + L_{\dot{\alpha}}}$

APPENDIX

Altitude-dependent derivatives	Conventional term	Wind shear contribution
A_{23}	$-\dfrac{L_q - mV_e}{mV_e + L_{\dot{\alpha}}}$	0
A_{24}	$-\dfrac{mg \sin \gamma_e}{mV_e + L_{\dot{\alpha}}}$	$\dfrac{mu_w' V_e \sin 2\gamma_e}{mV_e + L_{\dot{\alpha}}}$
A_{25}	0	$\dfrac{L_V + T_V \sin \alpha_T}{mV_e + L_{\dot{\alpha}}} u_w'$ (zero if $\gamma_e \neq 0$)
A_{31}	$\dfrac{1}{I_{yy}}\left(M_V - M_{\dot{\alpha}} \dfrac{L_V + T_V \sin \alpha_T}{mV_e + L_{\dot{\alpha}}}\right)$	$\dfrac{M_{\dot{\alpha}} mu_w' \sin^2 \gamma_e}{I_{yy}(mV_e + L_{\dot{\alpha}})}$
A_{32}	$\dfrac{1}{I_{yy}}\left(M_\alpha - M_{\dot{\alpha}} \dfrac{L_\alpha + T_e \cos \alpha_T - mg \sin \gamma_e}{mV_e + L_{\dot{\alpha}}}\right)$	$-\dfrac{M_{\dot{\alpha}} mu_w' V_e \sin^2 \gamma_e}{I_{yy}(mV_e + L_{\dot{\alpha}})}$
A_{33}	$\dfrac{1}{I_{yy}}\left(M_q + M_{\dot{\alpha}} \dfrac{mV_e - L_q}{mV_e + L_{\dot{\alpha}}}\right)$	0
A_{34}	$-\dfrac{M_{\dot{\alpha}} mg \sin \gamma_e}{I_{yy}(mV_e + L_{\dot{\alpha}})}$	$\dfrac{M_{\dot{\alpha}} mu_w' V_e \sin 2\gamma_e}{I_{yy}(mV_e + L_{\dot{\alpha}})}$
A_{35}	0	$-\dfrac{u_w'}{I_{yy}}\left(M_V - M_{\dot{\alpha}} \dfrac{L_V + T_V \sin \alpha_T}{mV_e + L_{\dot{\alpha}}}\right)$ (zero if $\gamma_e \neq 0$)
A_{41}	0	0
A42	0	0
A_{43}	1	0
A_{44}	0	0
A_{45}	0	0
A_{51}	$-\sin \gamma_e$	0
A_{52}	$V_e \cos \gamma_e$	0
A_{53}	0	0
A_{54}	$-V_e \cos \gamma_e$	0
A_{55}	0	0

APPENDIX

Altitude-dependent derivatives	Conventional term	Wind shear contribution
B_{11}	$\frac{1}{m}(\cos \alpha_T - D_{\delta T})$	0
B_{12}	$-\frac{1}{m} D_{\delta_e}$	0
B_{21}	$-\frac{\sin \alpha_T}{mV_e + L_{\dot{\alpha}}}$	0
B_{22}	$-\frac{L_{\delta_e}}{mV_e + L_{\dot{\alpha}}}$	0
B_{31}	$\frac{1}{I_{yy}}\left(M_{\delta T} - M_{\dot{\alpha}} \frac{\sin \alpha_T}{mV_e + L_{\dot{\alpha}}}\right)$	0
B_{32}	$\frac{1}{I_{yy}}\left(M_{\delta_e} - M_{\dot{\alpha}} \frac{L_{\delta_e}}{mV_e + L_{\dot{\alpha}}}\right)$	0
B_{41} to B_{52}	0	0

As mentioned in the section "Model Definition," the conventional derivatives were computed by the numerical differentiation technique described in reference 2. The terms containing u_w', the wind gradient, were computed using the above formulas. For that computation, the dimensional rotary stability derivatives $L_{\dot{\alpha}}$ and $M_{\dot{\alpha}}$ were needed. These quantities were obtained from their defining formulas:

$$L_{\dot{\alpha}} = qS \frac{\bar{c}}{2V_e} C_{L_{\dot{\alpha}}} \qquad \text{(where } C_{L_{\dot{\alpha}}} = -8\text{)}$$

$$M_{\dot{\alpha}} = qS \frac{\bar{c}^2}{2V_e} C_{m_{\dot{\alpha}}} \qquad (C_{m_{\dot{\alpha}}} = -2.65)$$

For the linear analysis, the linearized expression for the energy height rate was needed. This was approximated by

$$\dot{h}_e = \frac{V_e}{g} \frac{d}{dt}(\Delta V - \Delta Z_E)$$

APPENDIX

For the sake of completeness the numerical value of the A-matrix is given for values of u_w' equal to -1, 0, and 1:

$u_w' = -1$

-0.0459	11.67	0.0	-16.27	-0.0046
.0049	-.7080	.9990	.0	-.0003
.0024	-.4500	-.529	.0	.0003
.0	.0	1.0000	.0	.0
.0	64.92	.0	-64.92	.0

$u_w' = 0$

-0.0459	5.18	0.0	-9.81	0.0
-.0049	-.7080	.9999	.0	.0
-.0034	-1.4500	-.5290	.0	.0
.0	.0	1.0000	.0	.0
.0	64.92	.0	-64.92	.0

$u_w' = 1$

-0.0459	-1.29	0.0	-3.32	0.0046
.0049	-.7080	.9990	.0	.0003
.0023	-1.4500	-.5290	.0	.0003
.0	.0	1.0000	.0	.0
.0	64.92	.0	-64.92	.0

The B-matrix, whose elements do not depend on u_w', is also given:

0.0001	0.0
.0	-.0008
.0	-.0213
.0	.0
.0	.0

REFERENCES

1. Gera, Joseph: The Influence of Vertical Wind Gradients on the Longitudinal Motion of Airplanes. NASA TN D-6430, 1971.

2. Sherman, Windsor, L.: A Theoretical Analysis of Airplane Longitudinal Stability and Control as Affected by Wind Shear. NASA TN D-8496, 1977.

3. Etkin, Bernard: Dynamics of Atmospheric Flight. John Wiley & Sons, Inc., c.1972, pp. 154-163.

4. Dieudonne, James E.: Description of a Computer Program and Numerical Technique for Developing Linear Perturbation Models From Nonlinear Systems Simulations. NASA TM-78710, 1978.

5. Joppa, Robert G.: Wind Shear Detection Using Measurement of Aircraft Total Energy Change. NASA CR-137839, 1976.

6. Nicks, Oran W.: A Simple Total Energy Sensor. NASA TM X-73928, 1976.

7. Houck, Jacob A.: Operation and Evaluation of the Terminal Configured Vehicle Mission Simulator in an Automated Terminal Area Metering and Spacing ATC Environment. NASA Paper presented at the Summer Computer Simulation Conference (Toronto, Canada), July 16-18, 1979.

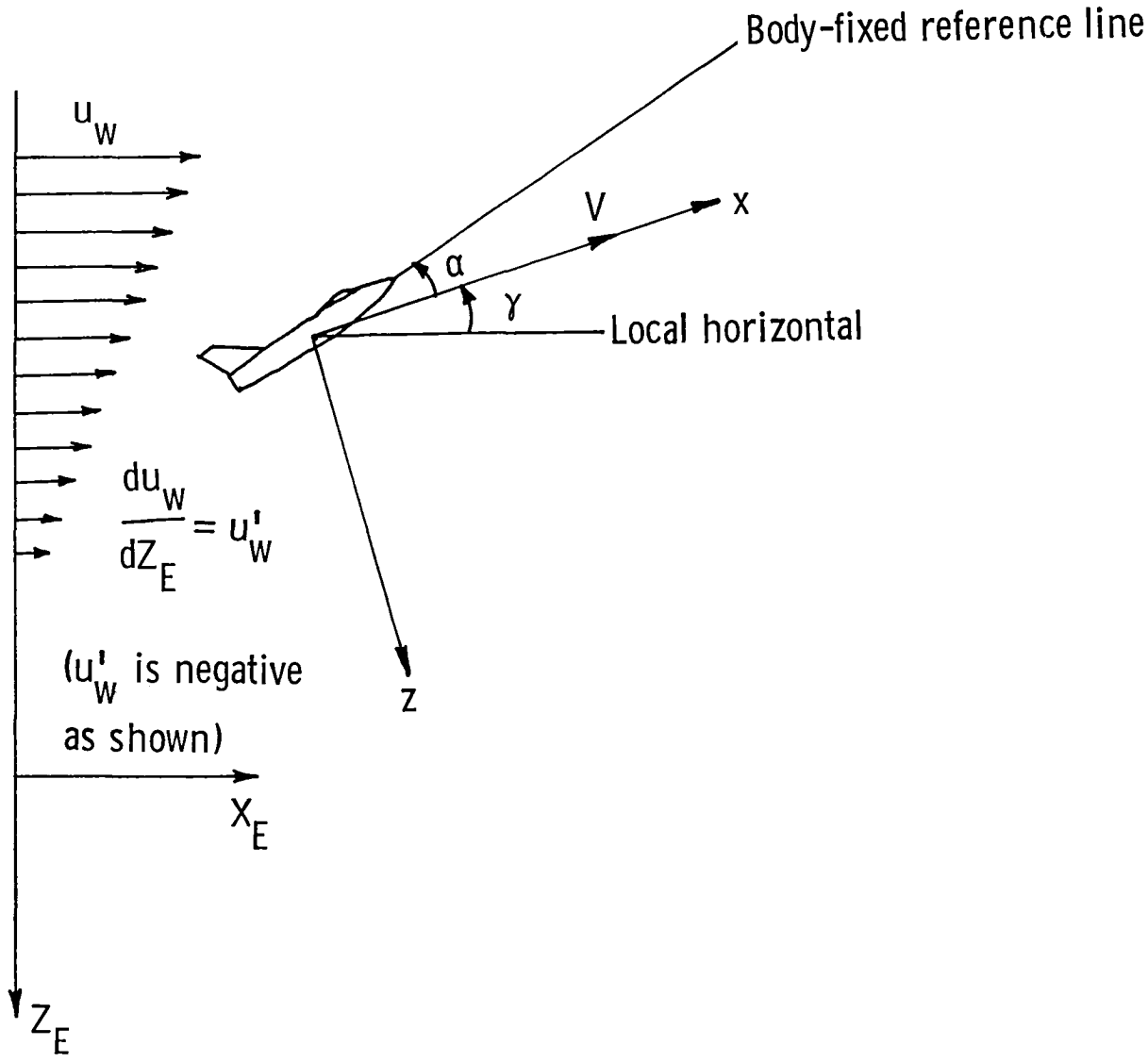

Figure 1.- Definition of Earth-fixed axes, moving axes, and wind gradient.

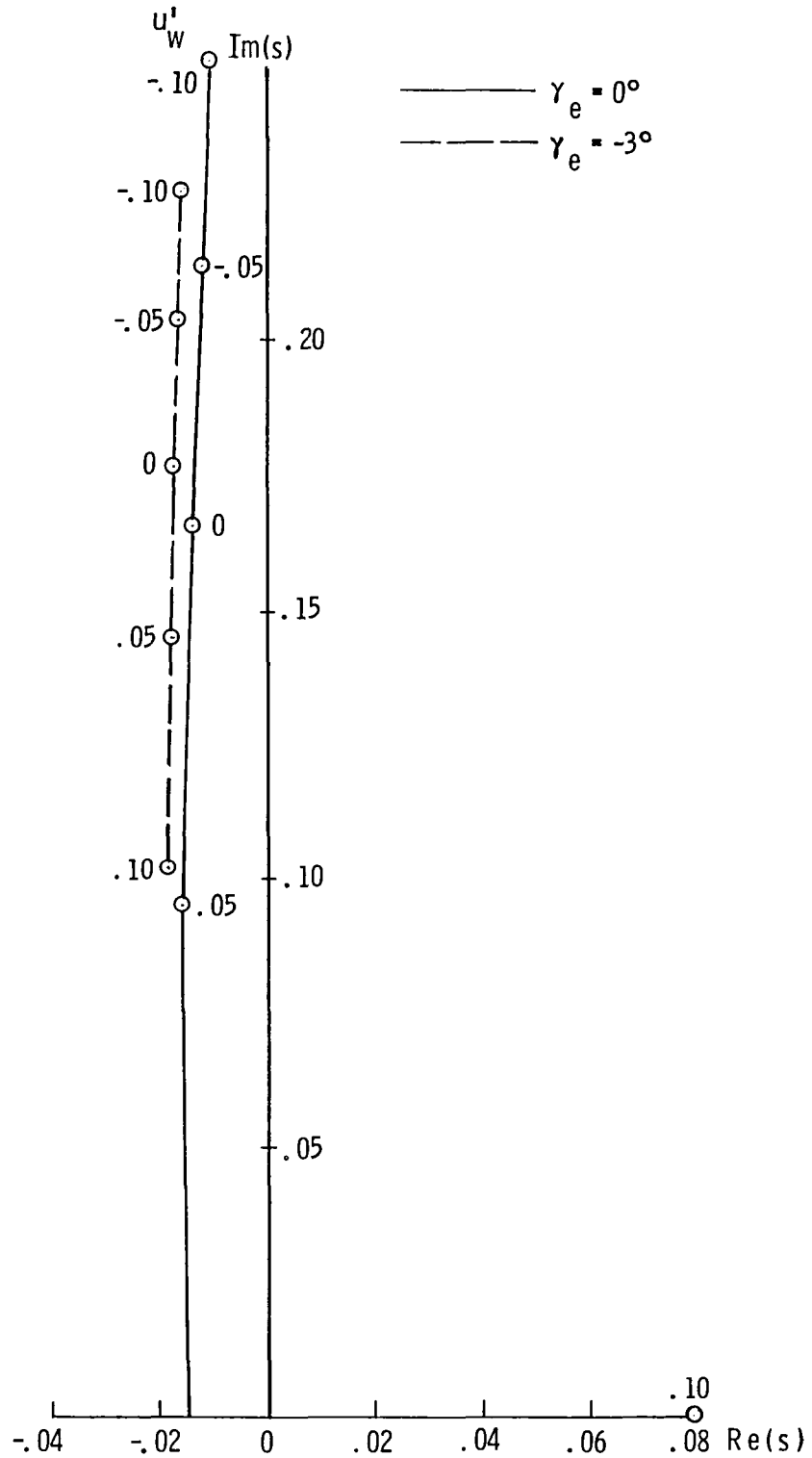

Figure 2.- Root contour plot showing effect of wind shear on phugoid motion.

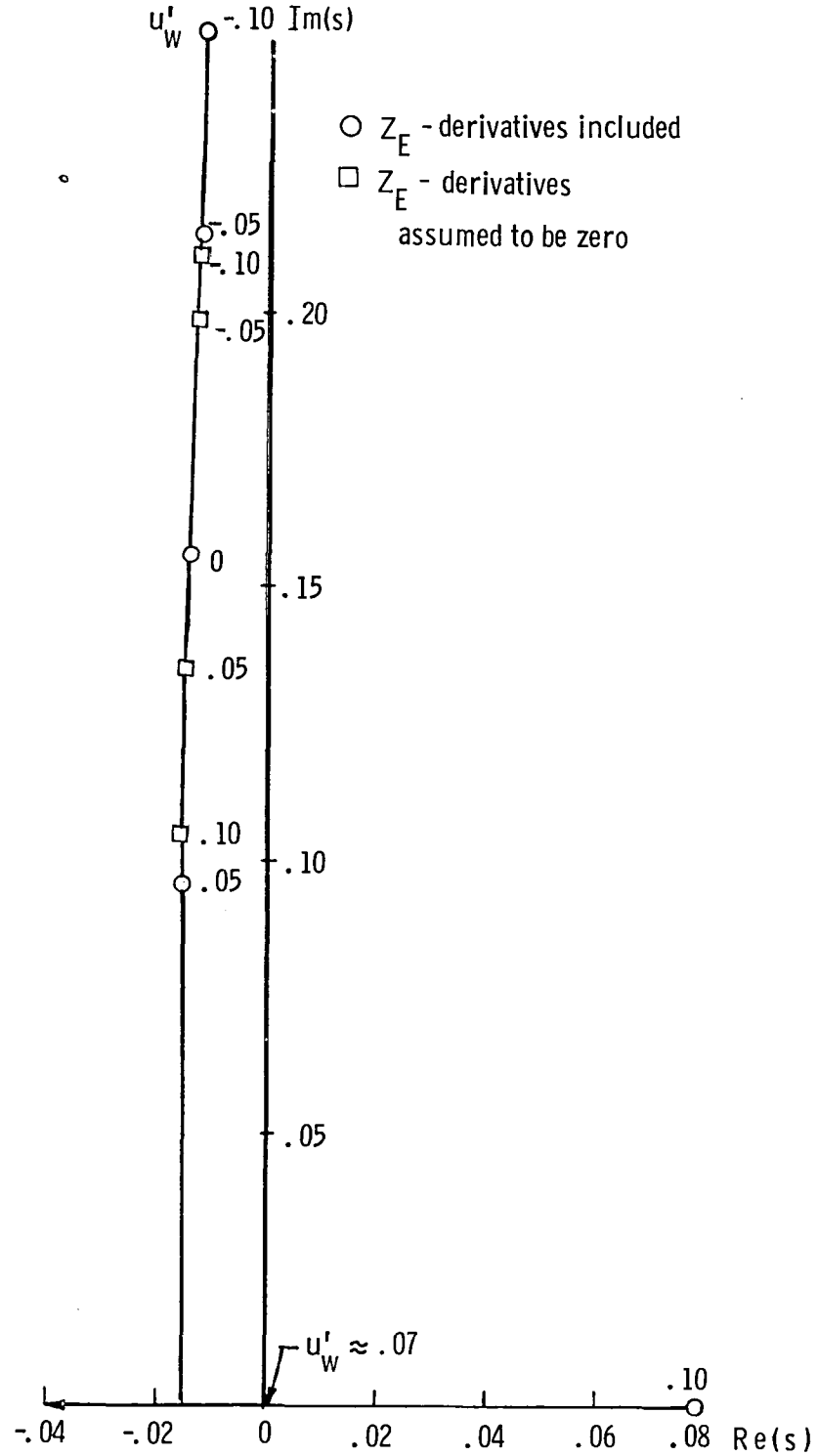

Figure 3.- Effect of Z_E-derivatives on $\gamma_e = 0$ root contour.

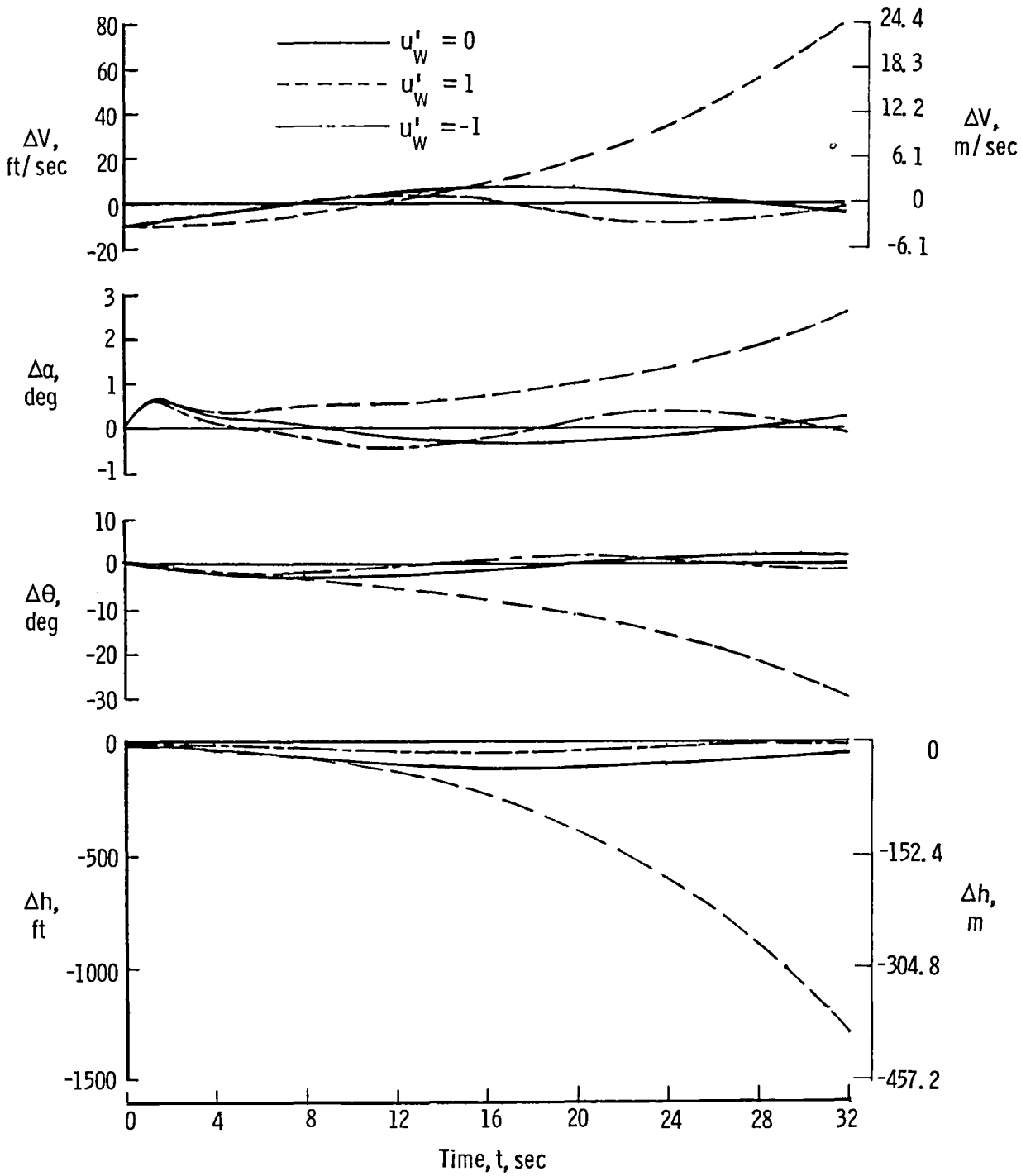

Figure 4.- Effect of wind shear on controls-fixed flight path after initial tail-wind gust of 3 m/sec.

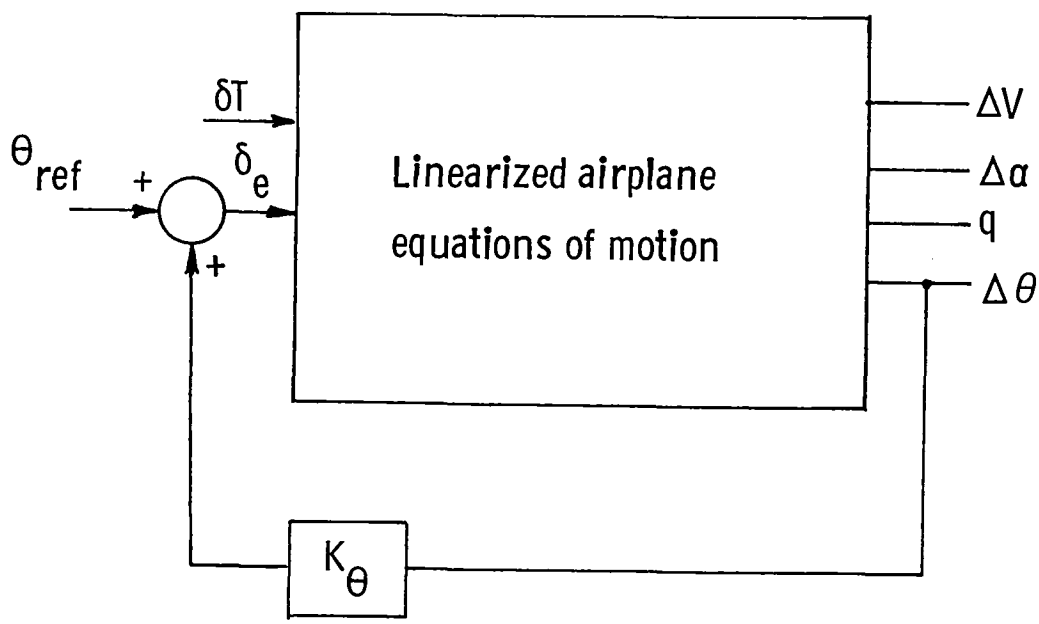

Figure 5.- Attitude control with feedback of pitch attitude to elevator.

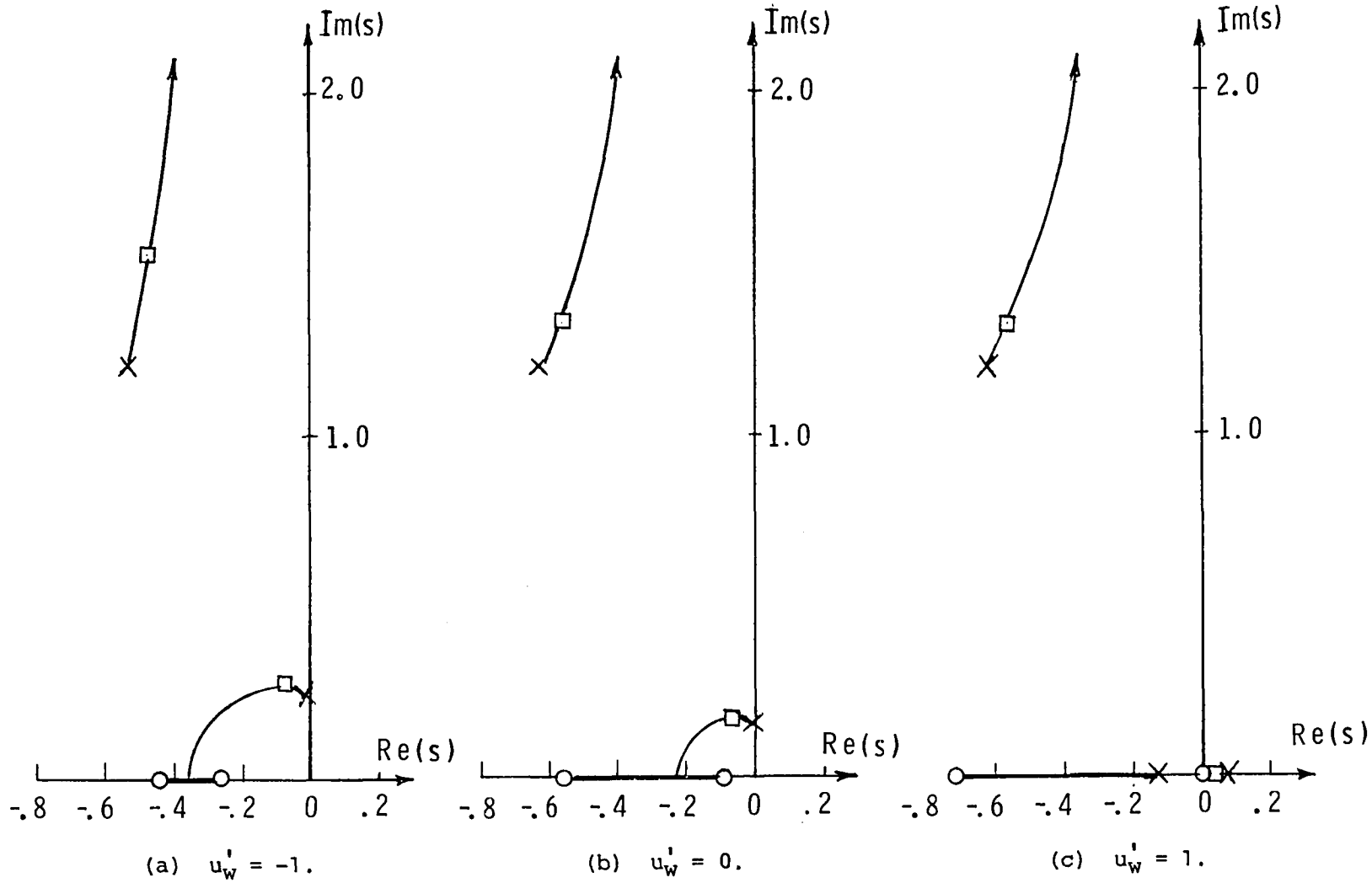

Figure 6.- Root locii showing effect of θ feedback to elevator.

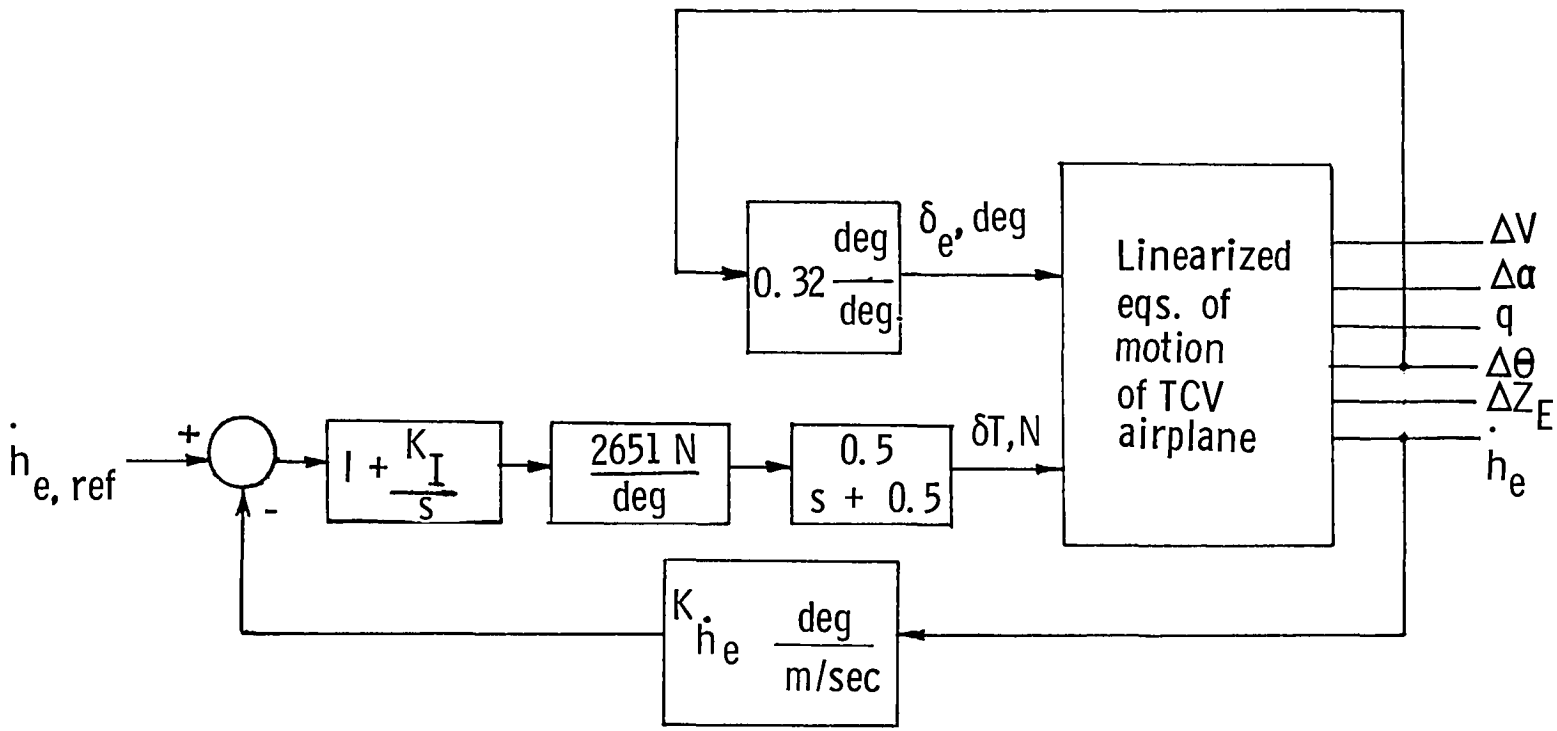

Figure 7.- Closed-loop control of linearized model of Terminal Configured Vehicle (TCV) airplane.

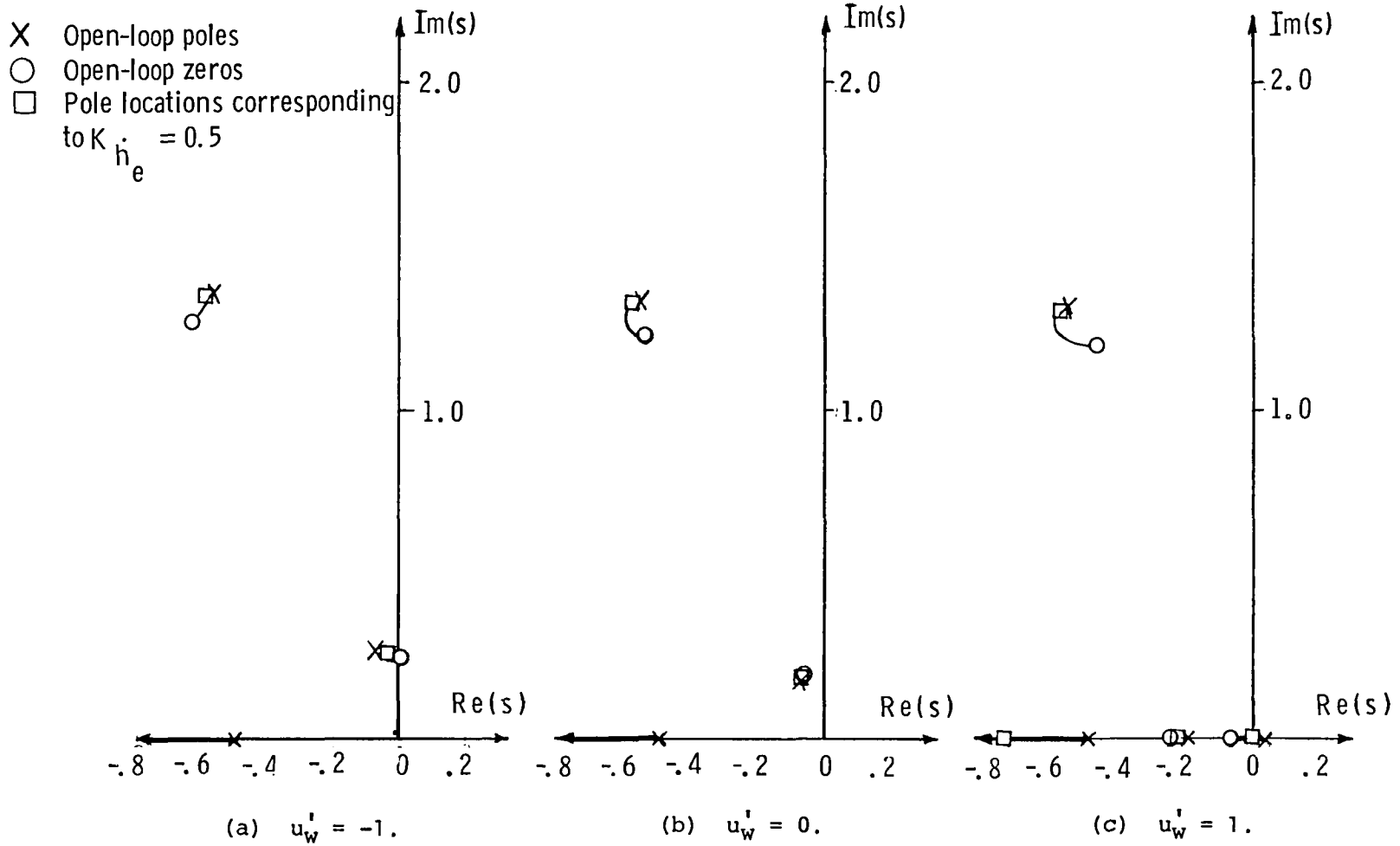

Figure 8.- Root locii showing effect of feedback to throttle. K_θ = 0.32 deg/deg.

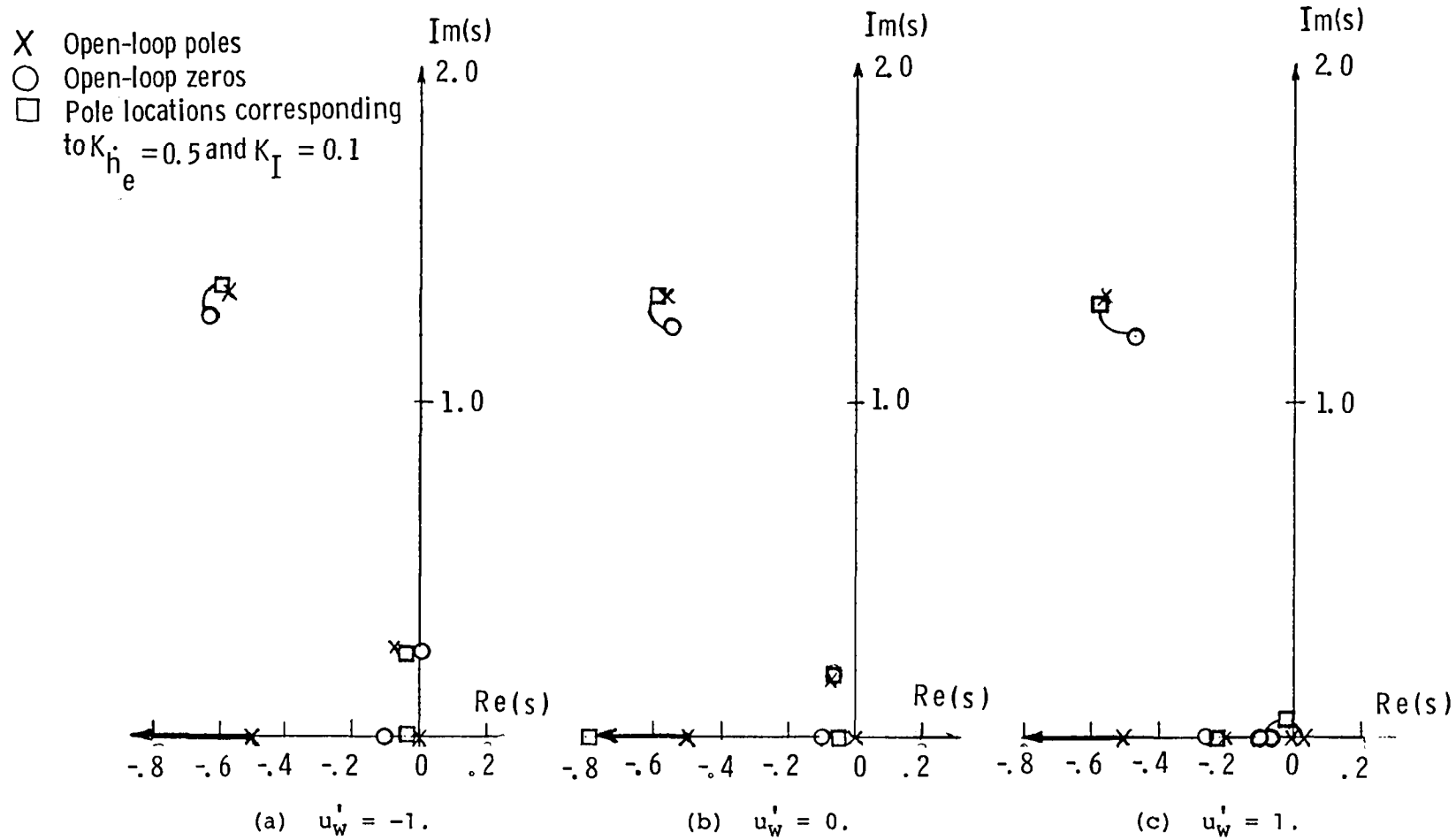

Figure 9.- Root locii showing effect of feedback.

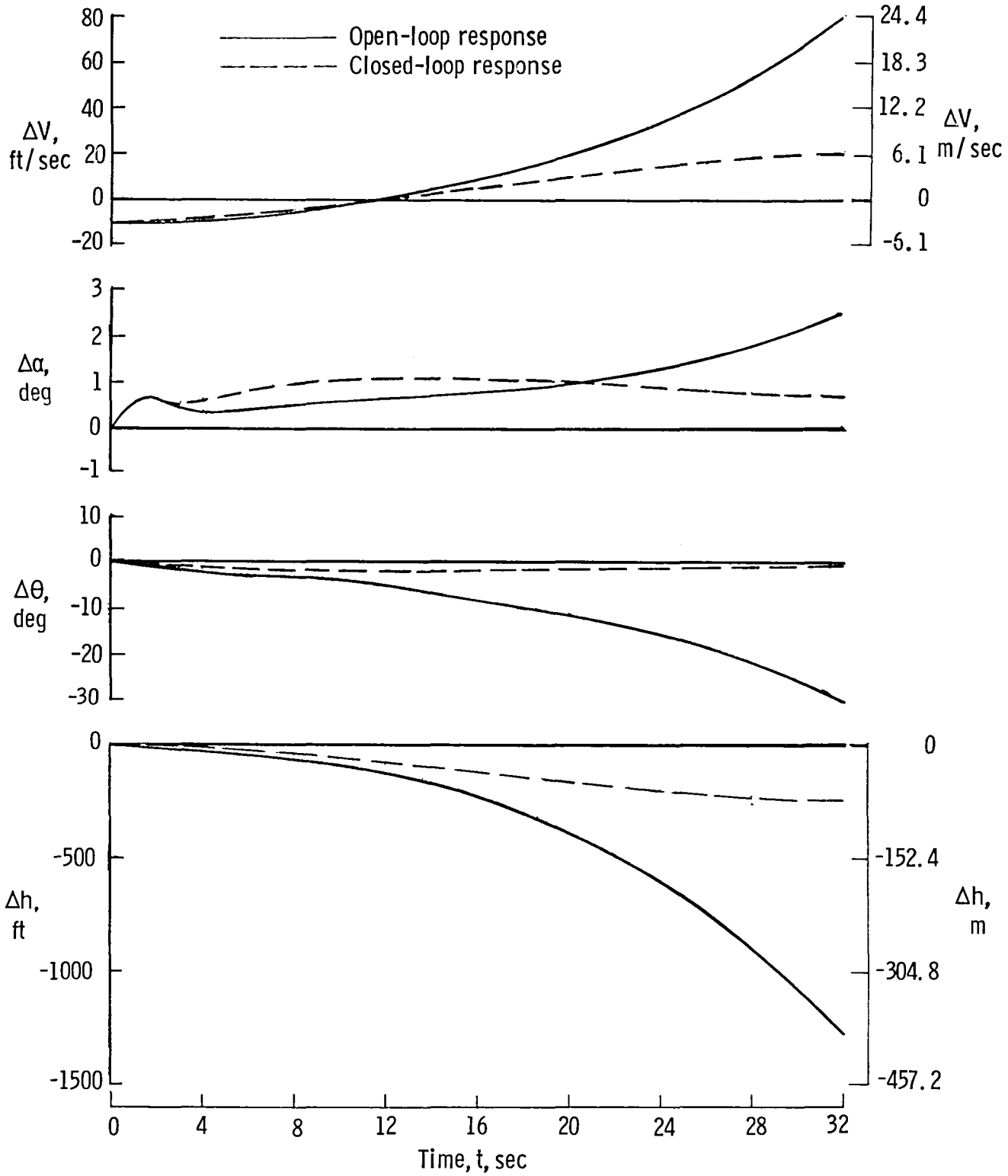

Figure 10.- Comparison of open- and closed-loop characteristics in wind shear $u_w' = 4$.

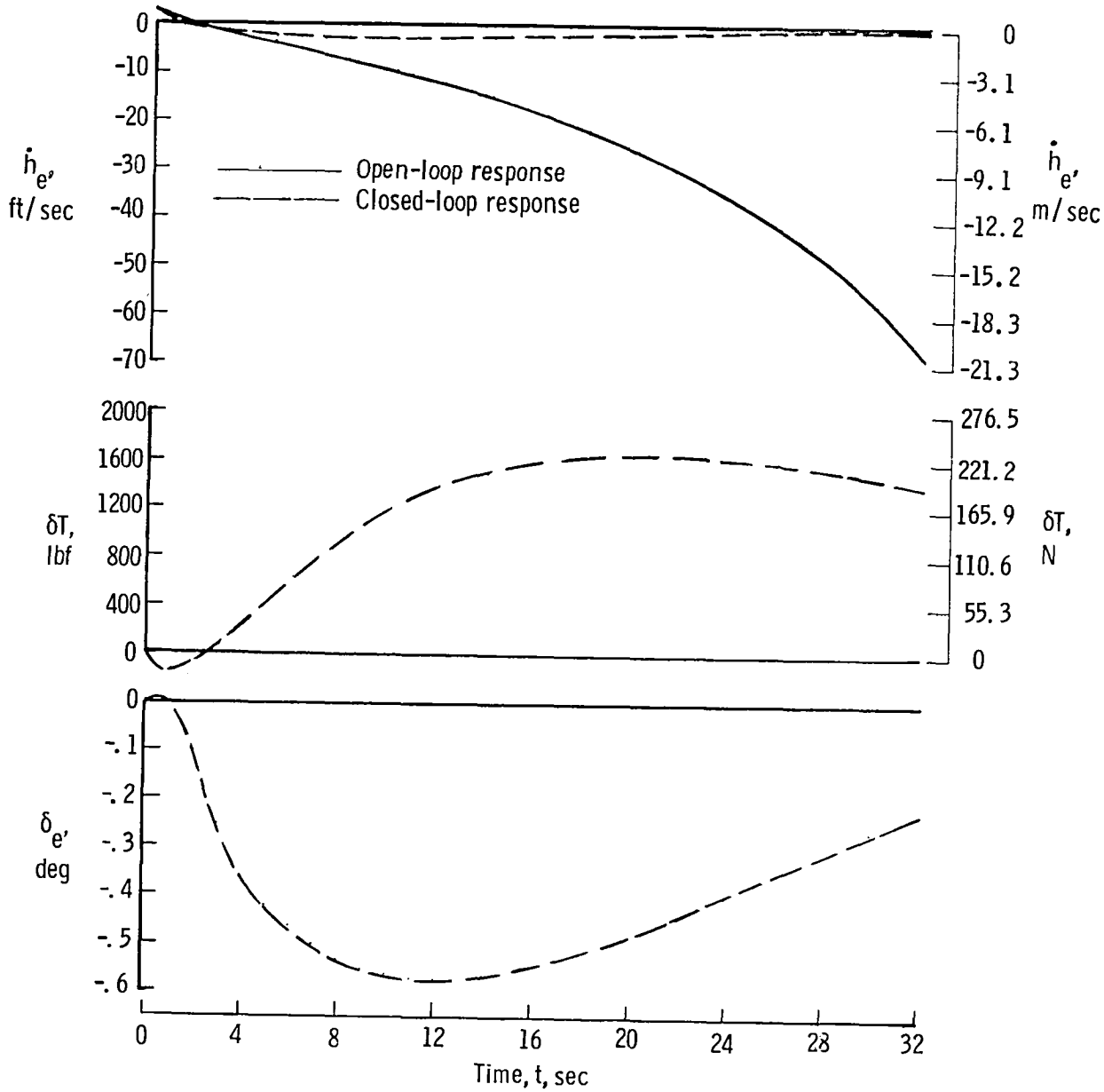

Figure 11.- Comparison of energy height rate and control response of open- and closed-loop system in wind shear $u_w' = 1$.

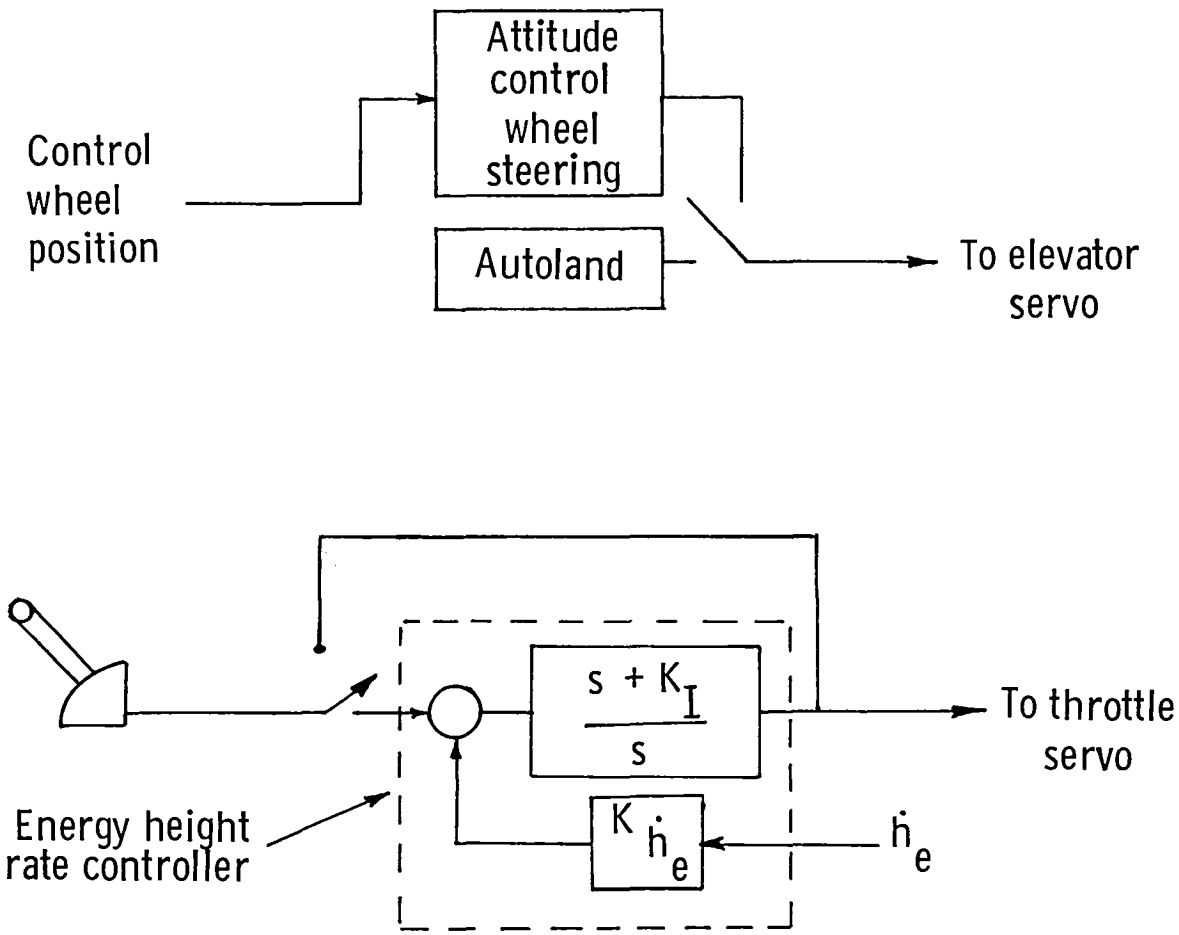

Figure 12.- Simplified schematic of simulation modes.

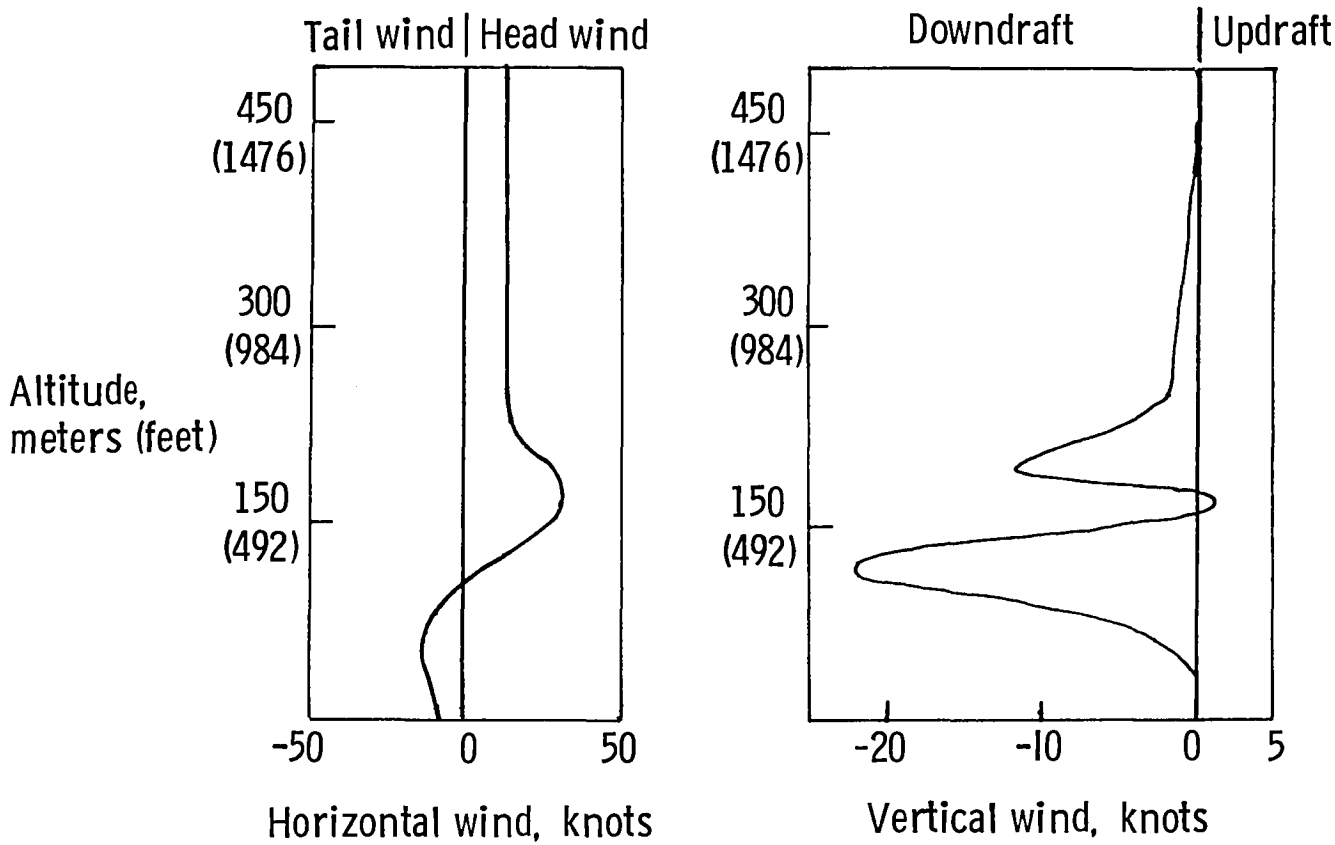

Figure 13.- Simulated wind profile.

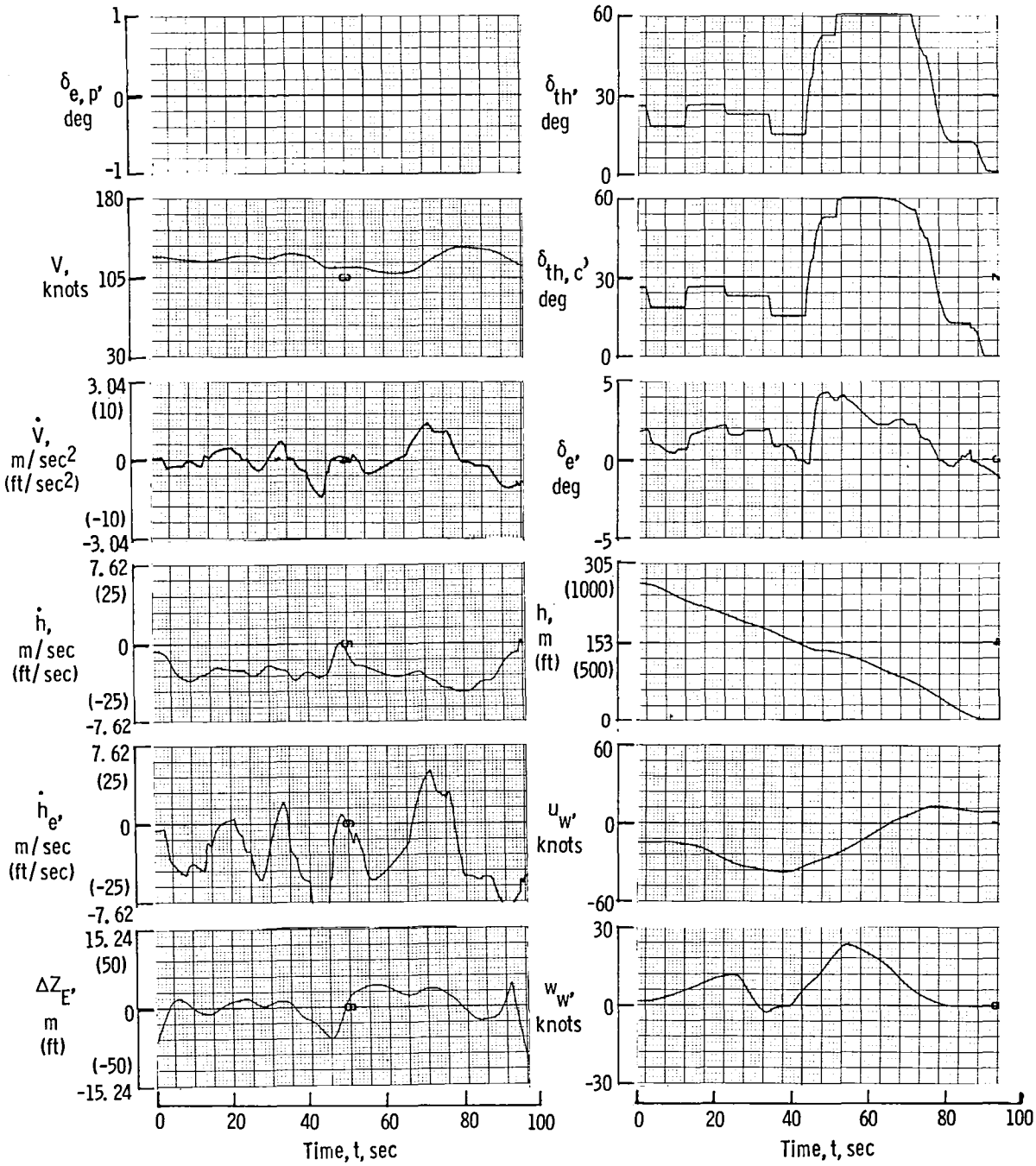

Figure 14.- Time history showing approach flown in wind shear with autoland and manual throttle.

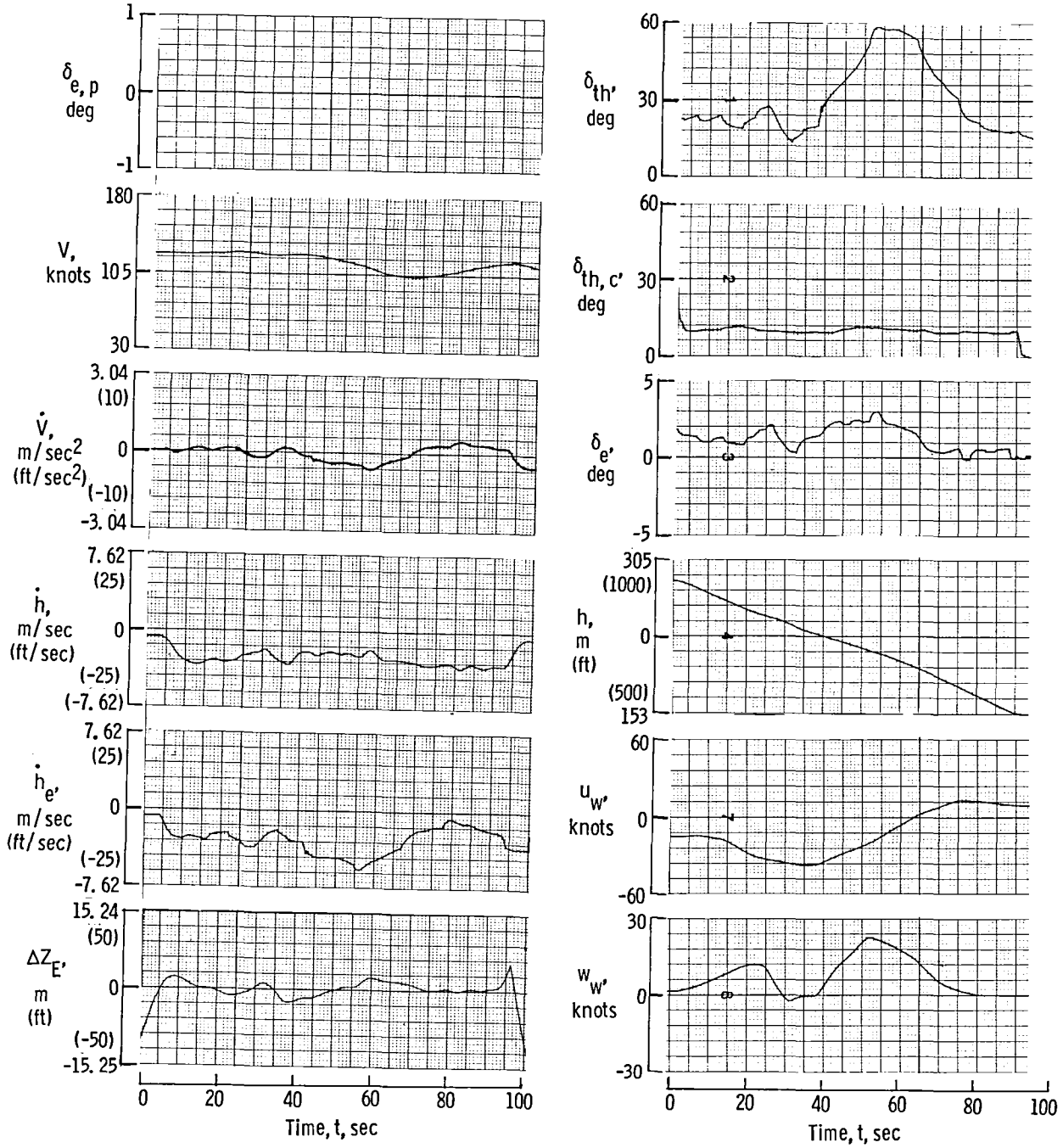

Figure 15.- Time history showing an approach flown in wind shear with autoland and energy height rate in throttle loop.

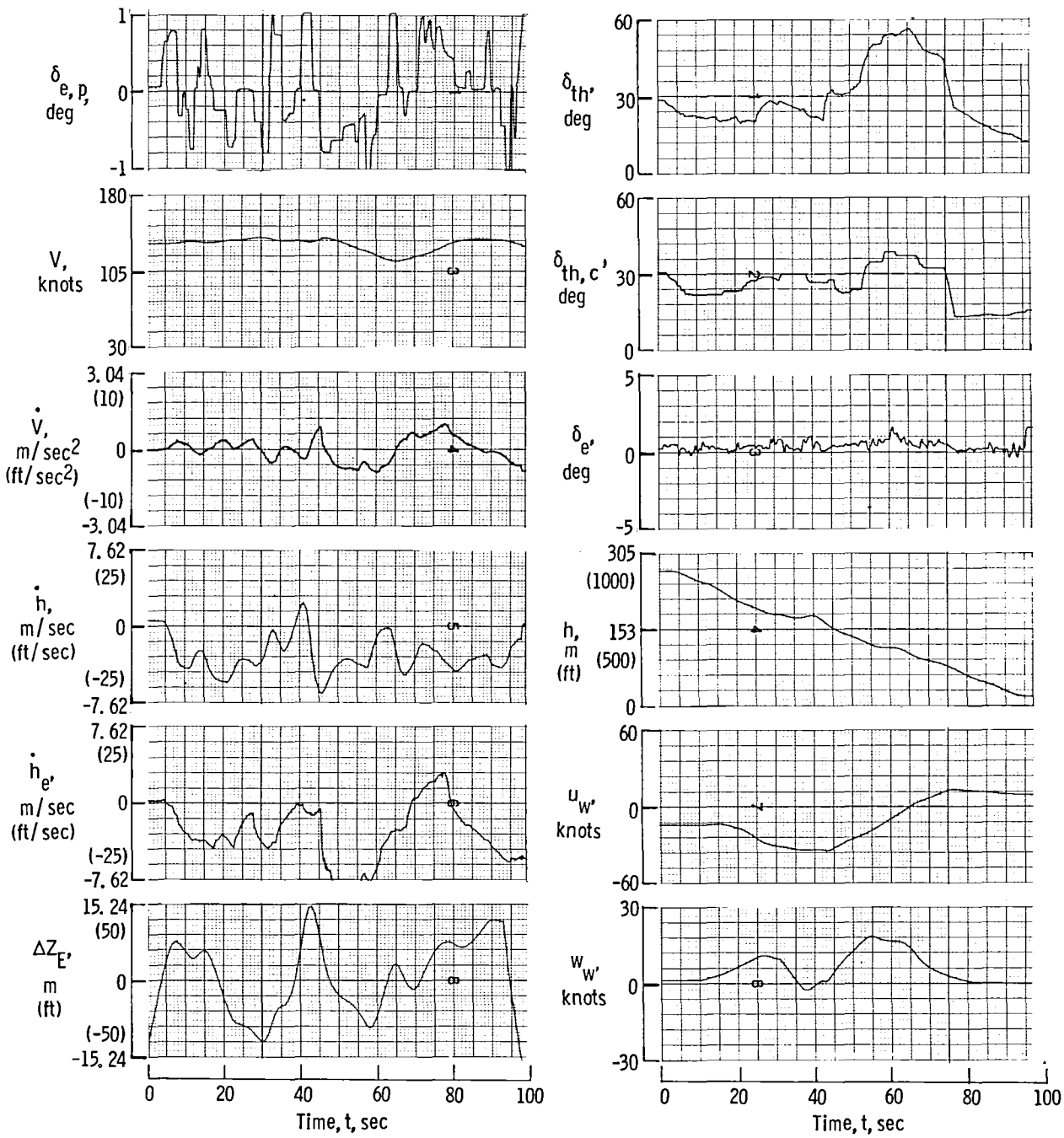

Figure 16.- Time history showing approach flow in wind shear with attitude-control-wheel steering in elevator loop and energy height rate feedback in throttle loop.

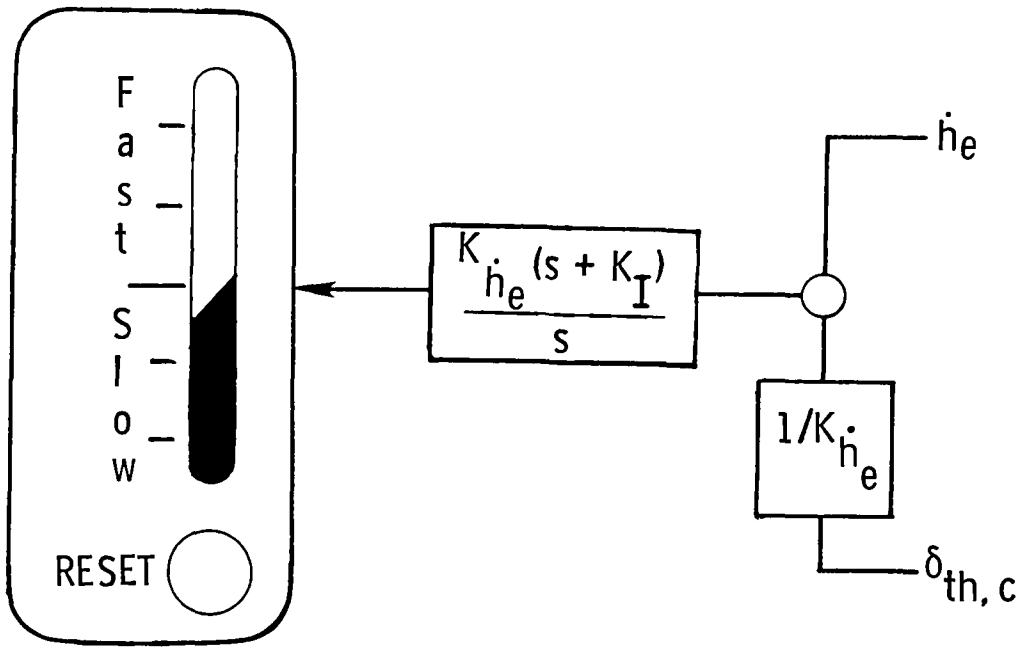

Figure 17.- Conceptual display of energy height rate to aid pilot in airplane energy management in wind shear.

1. Report No.	2. Government Accession No.	3. Recipient's Catalog No.
NASA TM-81828		

4. Title and Subtitle	5. Report Date
LONGITUDINAL STABILITY AND CONTROL IN WIND SHEAR WITH ENERGY HEIGHT RATE FEEDBACK	November 1980
	6. Performing Organization Code
7. Author(s)	8. Performing Organization Report No.
Joseph Gera	L-13130
	10. Work Unit No.
9. Performing Organization Name and Address	505-34-33-02
NASA Langley Research Center Hampton, VA 23665	11. Contract or Grant No.
	13. Type of Report and Period Covered
12. Sponsoring Agency Name and Address	Technical Memorandum
National Aeronautics and Space Administration Washington, DC 20546	14. Sponsoring Agency Code

15. Supplementary Notes

16. Abstract

The longitudinal linearized equations of motion in wind shear have been derived for the NASA Terminal Configured Vehicle, a modified Boeing 737 airplane. In addition to the apparent acceleration terms resulting from wind shear, the equations include altitude-dependent stability derivatives. A linear analysis of these equations indicates a first-order divergence type of instability due to wind shear in which head wind decreases with altitude. Furthermore, this instability cannot be stabilized by attitude control alone. However, attitude control used in combination with an additional feedback loop which consisted of the energy height rate feedback to the throttle proved to be effective in suppressing instability due to wind shear. A brief piloted, real-time, nonlinear simulation indicated the desirability of using a display based on the rate of change of energy height rate and of commanded thrust.

17. Key Words (Suggested by Author(s))	18. Distribution Statement
Wind shear effects Longitudinal stability and control Energy height rate	Unclassified - Unlimited Subject Category 08

19. Security Classif. (of this report)	20. Security Classif. (of this page)	21. No. of Pages	22. Price
Unclassified	Unclassified	37	A03

For sale by the National Technical Information Service, Springfield, Virginia 22161

NASA-Langley, 1980

National Aeronautics and
Space Administration

Washington, D.C.
20546

Official Business
Penalty for Private Use, $300

THIRD-CLASS BULK RATE

Postage and Fees Paid
National Aeronautics and
Space Administration
NASA-451

NASA

POSTMASTER: If Undeliverable (Section 158 Postal Manual) Do Not Return